CrystEngComm

PAPER

View Article Online
View Journal | View Issue

Cite this: *CrystEngComm*, 2017, **19**, 5422

A family of microscale 2 × 2 × 2 Pocket Cubes†

Minahi S. Aldossary,‡[a] Jian Zhu,‡[a] Rakesh R. Porob[b] and Da Deng *[a]

Hierarchical microscale materials have received much attention recently. They can find many important applications, including wastewater treatment and energy storage. However, it is still a challenging task to facilely synthesize microscale structures with good size distribution, unique structures and, particularly, tunable composition. Herein, we have prepared a family of 2 × 2 × 2 Pocket Cube-like hierarchical microparticles, with different chemical compositions, including bimetal hydroxide ($ZnSn(OH)_6$), mixed bimetal oxide and metal oxide (Zn_2SnO_4&SnO_2), carbon coated bimetal oxide and metal (Zn_2SnO_4&Sn@C), all with the same overall mesoscale microstructures. This family of microscale Pocket Cubes, with different chemical compositions and their associated different physiochemical properties, may offer a set of functional materials for many applications. In order to demonstrate their potential applications, we have preliminarily studied their performances in rechargeable batteries and water remediation. Interestingly, these selected Pocket Cubes are electrochemically active toward the reversible storage of both sodium and lithium with comparable performances to those nanoparticles reported, although their sizes are remarkably large on the microscale. We found that the shapes of the microparticles can influence their photocatalytic performances. Our preliminary results suggest that this family of microscale Pocket Cubes, with further optimization and improvement, can find many promising applications, including wastewater treatment and energy storage.

Received 22nd April 2017,
Accepted 3rd August 2017

DOI: 10.1039/c7ce00760d

rsc.li/crystengcomm

1. Introduction

Design and synthesis of microscale functional materials have been attracting much attention in recent years. Microscale functional materials, with tunable morphologies and structure dependent properties, may offer paradigm shifts in many applications, including energy storage,[1–3] wastewater treatment,[4] chemical sensors,[5–7] catalysis,[8] drug delivery,[9] *etc.* However, it is still a challenging task to facilely prepare a family of uniquely structured microscale materials with the same overall morphology and good size distribution, but with different chemical compositions. This family of microscale materials can offer customized materials, and their tunable properties can meet the requirements for various applications. Recently, significant progress has been achieved in the preparation of functional microscale materials. For example, CuO@ZnO microcubes were prepared *via* a two-step solution route and were proved to be the superior materials for p-type gas sensor application;[10] hollow $Li_{1.2}Mn_{0.5}Co_{0.25}Ni_{0.05}O_2$ microcubes were prepared *via* a template method and show good electrochemical performance as cathode materials for Li-ion batteries;[1] microstructured Zn_2SnO_4 was prepared by a hydrothermal method, demonstrating its improved photovoltaic and photoreduction performances.[11] We have been working on the design and synthesis of microscale materials for battery applications, including the microscale cubes of Zn_2SnO_4 based electrode materials, achieving improved volumetric capacities.[12]

Besides its application in batteries, the semiconductor Zn_2SnO_4, which has a band gap energy (E_g) of 3.6 eV (same as that of SnO_2),[13–15] can be potentially used in other applications, including photocatalysis.[8] Zn_2SnO_4 has been prepared by a hydrothermal method,[8] thermal evaporation method,[16] electrodeposition,[17] and high temperature solid-state reaction method.[18] Most of the reported Zn_2SnO_4 materials are on the nanoscale. Interestingly, the preparation of Zn_2SnO_4 on the microscale with good size distribution is relatively rare. It is still a challenging task to facilely prepare Zn_2SnO_4 with unique structure on the microscale under mild conditions. Given that Zn_2SnO_4 and SnO_2 have the same band gap, it is believed that their composite, Zn_2SnO_4/SnO_2, may offer new properties due to synergistic effects.[19] For example, Zn_2SnO_4/SnO_2 could have a lower band gap than pure Zn_2SnO_4.[20] Therefore, it will be interesting to explore facile procedures of

[a] *Department of Chemical Engineering and Materials Science, Wayne State University, Detroit, Michigan, 48202, USA. E-mail: da.deng@wayne.edu*
[b] *Department of Chemistry, Wayne State University, 5050 Anthony Wayne Dr, Detroit, Michigan, 48202, USA*

† Electronic supplementary information (ESI) available: TGA of $ZnSn(OH)_6$ in argon; additional FESEM images; UV-vis absorption spectra and C/C_0 of MB without a catalyst under the exposure to UV-light; Li-ion battery test of ZTO&SnO_2 and ZTO&Sn@C. See DOI: 10.1039/c7ce00760d

‡ Aldossary and Zhu contributed equally.

synthesizing Zn_2SnO_4/SnO_2 based microscale composites and their derivatives.

Herein, we report the facile synthesis of a family of Pocket Cube-like microstructures *via* a simple procedure. We demonstrate that Pocket Cubes of (1) crystalline $ZnSn(OH)_6$, (2) mixed metal oxide Zn_2SnO_4&SnO_2 nanoparticles as the building units, (3) mixed metal oxide and a metal encapsulated in carbon Zn_2SnO_4&Sn@C nanoparticles as the building units, and (4) carbon bubbles as the basic building units could be facilely prepared. This family of Pocket Cubes, with different chemical compositions but with similar microscale structures, can offer a series of microscale materials for potential applications. We preliminarily demonstrated that this family of Pocket Cubes, although on the microscale instead of nanoscale, can be employed for energy storage in rechargeable lithium and sodium ion batteries, and as photocatalysis for water treatment.

2. Experimental section

Preparation of Pocket Cubes of $ZnSn(OH)_6$

The Pocket Cubes of $ZnSn(OH)_6$ particles were synthesized by co-precipitation at room temperature. Typically, a calculated amount of $ZnCl_2$ and $SnCl_4$ was added into 50 mL ethanol under stirring, forming a solution with a concentration of 0.025 M and 0.045 M for $ZnCl_2$ and $SnCl_4$, respectively. Then, 50 mL NaOH aqueous solution (0.32 M) was added into the mixed solution dropwise under vigorous stirring. After further stirring for one hour, the solution was maintained at room temperature for 24 hours without stirring. A white precipitate was collected by centrifugation and washed with water and ethanol three times to remove any residual ions. The $ZnSn(OH)_6$ precursor powder was then dried in a conventional oven at 100 °C overnight.

Preparation of Pocket Cubes of Zn_2SnO_4&SnO_2

Typically, the Pocket Cubes of the $ZnSn(OH)_6$ precursor were heated at 800 °C at a ramping rate of 20 °C min^{-1} in air to obtain the Pocket Cubes of Zn_2SnO_4&SnO_2 nanoparticle aggregates.

Preparation of Pocket Cubes of Zn_2SnO_4&Sn@C

The Pocket Cubes of Zn_2SnO_4&SnO_2 were treated by chemical vapor deposition (CVD) at 650 °C for 1 h in a tube furnace with a flow of mixture gas (10% acetylene as the carbon source balanced by argon) at 100 sccm to obtain the Pocket Cubes of Zn_2SnO_4&Sn@C. Acetylene can reduce SnO_2 into metallic Sn, which is well documented. Argon was used in the heating and cooling processes.

Preparation of Pocket Cubes of C nanobubbles

Pocket Cubes of C nanobubble assemblies were prepared by removing the carbon encapsulated Zn_2SnO_4&Sn nanoparticles from concentrated HCl acid (12 M) for 2 days and thoroughly washed.

Materials characterization

X-ray diffraction (XRD) was carried out using a Rigaku SmartLab X-ray diffractometer, with Cu Kα radiation (λ = 0.15418 nm) at a scanning speed of 4.0 degrees per minute. The morphology of the products was characterized using field emission scanning electron microscopy (JSM-7600 FESEM, equipped with Pegasus Apex 2 integrated EDS, with an accelerating voltage of 15 kV) and by transmission electron microscopy (JEOL 2010 TEM instrument, with an accelerating voltage of 200 kV). Thermo-gravimetric analysis (TGA) was performed under an argon atmosphere at a heating rate of 10 °C min^{-1} (TA instrument SDT Q600).

Evaluation of photocatalytic activity

Methylene blue (MB), as the model for organic chemical contaminant, was dissolved in DI-water to prepare a blue color aqueous solution (6 μM). 60 ml of the MB solution was stirred for 10 minutes in the dark before adding the catalysts. Then, 60 mg of the as prepared Zn_2SnO_4&SnO_2 microparticle powder was added into the solution and stirred for 15 min in the dark to establish the adsorption and desorption equilibrium. The mixture was kept stirring for the entire experiment. At time zero (after the equilibrium was established), the photocatalytic treatment was started by turning on the UV light (ACE photochemical apparatus equipped with a 450 watt UV light source). 2 mL of the solution under the exposure to UV light was taken out every three minute and analyzed using UV-vis spectrophotometers (Shimadzu2600) and poured back after the measurement.

Evaluation of electrochemical performance

For Na-ion batteries, the as-prepared Pocket Cubes of carbon bubbles as the building units (90 wt%) were mixed with 10 wt% of polyvinylidene fluoride (PVDF) in *N*-methylpyrrolidone (NMP) to prepare a slurry. Note: no carbon black as a conductivity enhancer was used. The slurry was coated on a Cu disc current collector. The coated Cu disc was dried in a vacuum oven at 80 °C overnight. The as-prepared electrodes as the working electrodes were assembled in CR2032 coin-type cells in an argon-filled glove box, with a metallic Na disc as the counter electrode, $NaClO_4$ (1 M) in a mixture of ethylene carbonate (EC) and diethyl carbonate (DEC) (1 : 1, v/v) as the electrolyte, and a Celgard 3501 PP membrane as the separator. The as-assembled Na-ion batteries were tested galvanostatically at room temperature, with a cut-off voltage range of 0.005–2 V at currents from 25 to 300 mA g^{-1} using an MTI BST8-WA battery tester. Tests for the performances in lithium-ion batteries were carried out similarly.

3. Results and discussion

3.1. Formation of a family of 2 × 2 × 2 Pocket Cubes with different compositions

The overall idea and the procedure under the experimental conditions involved in each step are illustrated in Scheme 1.

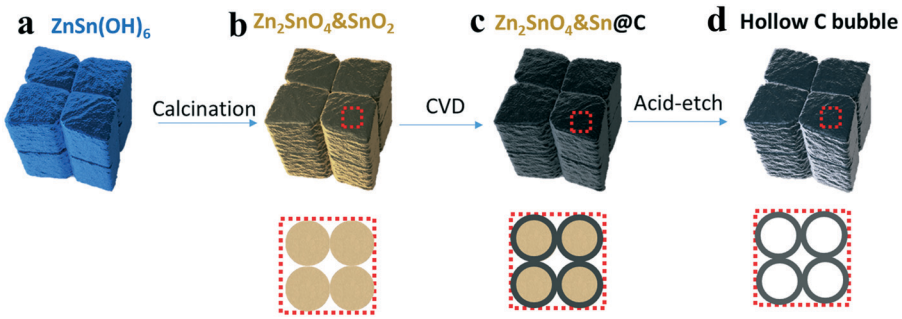

Scheme 1 Schematic of the flow chart for the synthesis of a family of Pocket Cubes with different compositions and building units: Pocket microcubes of (a) $ZnSn(OH)_6$ prepared by co-precipitation, (b) mixed oxides of Zn_2SnO_4&SnO_2 obtained by calcinating (a) in air, (c) Zn_2SnO_4&Sn@C obtained by the CVD treatment of (b), and (d) hollow carbon nanobubble assemblies obtained by the acid-removal of the Zn_2SnO_4&Sn core from (c). Their nanosized building units were enlarged beneath those microparticles to illustrate their porous nature.

The Pocket Cubes of $ZnSn(OH)_6$ were prepared without any surfactants *via* a simple co-precipitation method. This method could easily produce grams of Pocket Cube $ZnSn(OH)_6$ microparticles at room temperature. Simple calcination in air could convert $ZnSn(OH)_6$ to Zn_2SnO_4&SnO_2 *via* dehydration. The CVD treatment using acetylene as the carbon source and reducing agent under the protection of argon could achieve good encapsulation of the Zn_2SnO_4&Sn in carbon shells, where the metallic Sn was reduced from SnO_2 under CVD conditions. Carbon nanobubble aggregation was obtained *via* the removal of the Zn_2SnO_4&Sn core by acid wash. All the family members have the same microscale Pocket Cube-like structures.

The chemical compositions of those selected family members of the Pocket microcubes were characterized by XRD (Fig. 1). All the diffraction peaks could be assigned to $ZnSn(OH)_6$ (JCPDS card no. 20-1455) with no other peaks (Fig. 1a), indicating the successful formation of the $Pn\bar{3}m$ cubic phase $ZnSn(OH)_6$ with high purity. No impurity peaks associated with Zn $(OH)_2$, $Sn(OH)_4$, ZnO, or SnO_2 were determined, suggesting that our formulated alkaline environment using an excess amount of OH^- and room temperature reactions could help to avoid the formation of those impurities. The simple reaction can be described as:

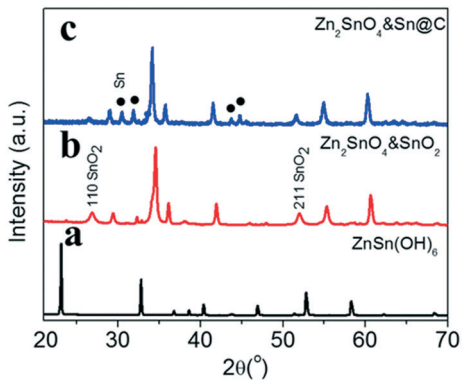

Fig. 1 XRD patterns of the Pocket Cubes of the (a) $ZnSn(OH)_6$ precursor, (b) Zn_2SnO_4&SnO_2 particle aggregates obtained *via* calcination of (a), and (c) Zn_2SnO_4&Sn@C obtained *via* the CVD treatment of (b).

$$Sn^{4+}_{(aq)} + Zn^{2+}_{(aq)} + 6OH^-_{(aq)} \rightarrow ZnSn(OH)_6\downarrow \quad (1)$$

In Fig. 1(b), all diffraction peaks in the XRD pattern for the calcinated sample can be assigned to the $Fd\bar{3}m$ cubic phase Zn_2SnO_4 (JCPDS card no. 24-1470) and $P42/mnm$ tetragonal phase SnO_2 (JCPDS card no. 41-1445). XRD analysis suggests the complete conversion of $ZnSn(OH)_6$ into Zn_2SnO_4 and SnO_2 under heat treatment. The reaction is as follows:

$$2ZnSn(OH)_6 \rightarrow Zn_2SnO_4 + SnO_2 + 6H_2O \quad (2)$$

The TGA analysis of the precursor, the Pocket Cubes of $ZnSn(OH)_6$, from room temperature to 900 °C range at a heating rate of 10 °C min^{-1}, further confirmed the as-proposed decomposition reaction (2) under heat treatment (Fig. S1 in the ESI†). The TGA curve involves an initial weight loss of 1.8 wt% below 200 °C corresponding to the removal of the absorbed and adsorbed water and ethanol. After the initial weight loss, a sharp decrease in the mass starting at ~200 °C and ending at ~280 °C was observed, which could represent the dehydration of the precursor, $ZnSn(OH)_6$, with the loss of water. The total weight loss between 200 °C to 600 °C was calculated to be 19.26 wt%, which agrees closely with the theoretical weigh loss (18.87 wt%) of reaction (2). Therefore, the TGA analysis also indirectly evidenced that the as-prepared Pocket Cubes of $ZnSn(OH)_6$ is highly phase pure.

In Fig. 1(c), the XRD patterns of the Pocket Cubes of Zn_2SnO_4&Sn@C obtained through the CVD treatment of Zn_2SnO_4&SnO_2 under acetylene clearly show the presence of metallic Sn. The distinguishable peak at around 26°, for SnO_2 (110) in Fig. 2(b), almost disappeared after the CVD treatment. Instead, the characteristic peaks at 31° and 32° associated with metallic Sn (JCPDS card no. 04-0673) appeared after the CVD treatment. This suggests that SnO_2 was reduced to Sn by acetylene through the CVD process. Acetylene with reducing capacity can transform SnO_2 into metallic Sn under such CVD conditions.[21–23] No peak of carbon was observed, indicating that the as-coated carbon was mainly amorphous. Based on the broadness of the diffraction peaks, the grain sizes of those samples can be roughly estimated using the Scherrer equation. The estimated crystalline size

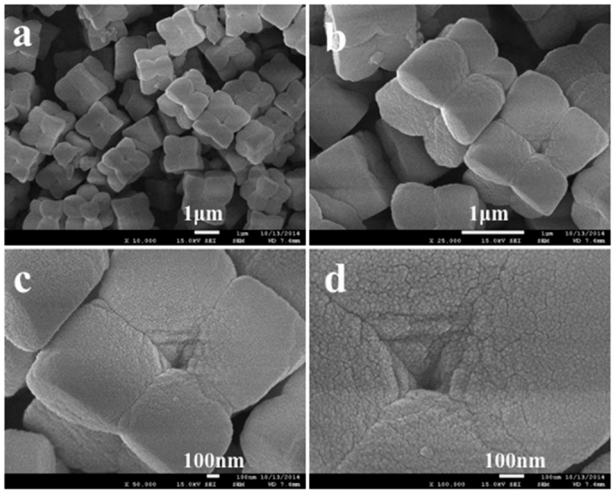

Fig. 2 FESEM images of the $ZnSn(OH)_6$ Pocket Cube precursor prepared *via* co-precipitation at different magnifications: (a) overall-view, (b) a few representative Pocket Cubes, (c) single Pocket Cube showing the detailed structure and (d) high-magnification image showing the building units.

for the Pocket Cubes of $ZnSn(OH)_6$ after co-precipitation is about 50 nm; after calcination, Zn_2SnO_4 and SnO_2 have a size of 23 nm and 13 nm, respectively; and after the chemical vapor deposition treatment, Zn_2SnO_4 and Sn have a size of 27 nm and 19 nm, respectively.

3.2. Morphology of the 2 × 2 × 2 Pocket Cubes of $ZnSn(OH)_6$

The morphology and sizes of the Pocket Cubes of the $ZnSn(OH)_6$ precursor particles were thoroughly characterized by FESEM, as shown in Fig. 2. The low-magnification FESEM images clearly show the unique microscale structures, similar to Pocket Cubes, with 8 corners. The average size is approximately 1.5 μm (Fig. 2a and b). A cave at the center of one facet of the Pocket Cube structure was observed (Fig. 2c). To the best of our knowledge, this unique Pocket Cube-like structure of $ZnSn(OH)_6$ with a microscale size has not been reported before. Most of the reported $ZnSn(OH)_6$ have spherical or polyhedral structures, such as cube and octahedrons, and typically have nanoscale sizes.[24,25] The surface of the $ZnSn(OH)_6$ precursor is relatively smooth on the microscale (Fig. 2d). Microparticles with sharper features of Pocket Cubes were observed (Fig. S2 in the ESI†). The Pocket Cubes with different degrees of maturity were observed as well (Fig. S3 in the ESI†).

3.3. Tuning the morphologies of the $ZnSn(OH)_6$ microparticles

Experimentally, we could tune the morphologies of those microparticles by changing the experimental conditions. For example, microsized particles with the shapes of cube, truncated cube, cubic frame and Pocket Cube were successfully synthesized (Fig. 3). At low concentrations of $SnCl_4$ at 0.025 M and $ZnCl_2$ at 0.05 M but with an abundant concentration of NaOH at 0.32 M, mesocubes were formed (Fig. 3a).[12] When the concentrations of $SnCl_4$ and $ZnCl_2$ were further reduced, truncated mesocubes were formed (Fig. 3b). Dashed lines are provided to highlight the features of the truncated cubes in Fig. S6 in the ESI.† The formation of truncated mesocubes could be considered to be because the corners were etched off by OH^- to minimize the surface energy or attributed to the slow growth in the vertices. As compared to those mesocubes, smaller particles were observed on the surface of those truncated mesocubes. Interesting cubic mesoframes were formed when the concentration of $ZnCl_2$ was decreased while the concentration of $SnCl_4$ was unchanged (Fig. 3c). When the concentration of $SnCl_4$ was increased while the concentration of $ZnCl_2$ was unchanged, Pocket mesocubes were formed (Fig. 3d). In order to clearly show the structural features of those microparticles observed by SEM, we tried to provide illustrations beneath each SEM image of the particles, as shown in Fig. 3. It should be noted that the illustrations may not precisely resemble the detailed morphologies of those particles but they do clearly outline their main features in terms of their overall morphology differences.

The morphology differences observed could be rationalized. With the abundance of NaOH, the presence of soluble $Zn[(OH)_4]^{2-}$ and $Sn[(OH)_6]^{2-}$ was expected in the case of the excess amount of $ZnCl_2$ and $SnCl_4$ used, respectively, .[24] $ZnSn(OH)_6$ can be selectively etched if excessive amounts of OH^- exist in the reaction system for a prolonged time.[26]

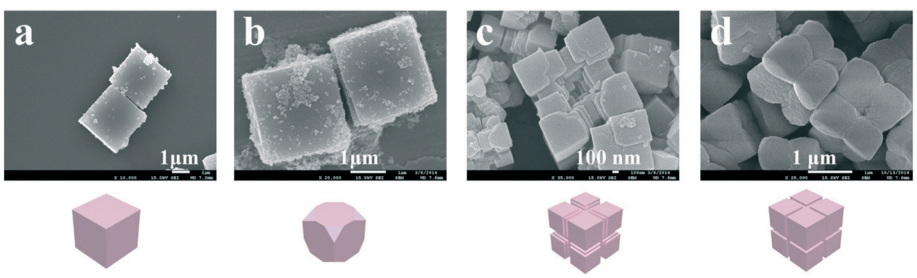

Fig. 3 Morphology of $ZnSn(OH)_6$ could be tuned by changing the experimental conditions: (a) mesocubes; synthesis conditions: $SnCl_4$, 0.025 M; $ZnCl_2$, 0.05 M; NaOH, 0.32 M; time, 23 h. (b) Truncated mesocubes; synthesis conditions: $SnCl_4$, 0.017 M; $ZnCl_2$, 0.025 M; NaOH, 0.32 M; time, 2 h. (c) Cubic frames; synthesis conditions: $SnCl_4$, 0.025 M; $ZnCl_2$, 0.025 M; NaOH, 0.32 M; time, 2 h. (d) Pocket mesocubes; synthesis conditions: $SnCl_4$, 0.045 M; $ZnCl_2$, 0.025 M; NaOH, 0.32 M; time, 24 h.

Those species could interact with the surface of the microparticles and change their surface energy, leading to the formation of different morphologies. At the same time, different supersaturations at the growth front also lead to the anisotropic growth forming different morphologies. The preliminary experimental results suggest that one can finely control and tune the morphologies of the final products by controlling the experimental conditions, including time, concentration, and temperature. Those series of samples will provide good models to investigate the structure–property relationships, particularly the effects of different exposed facets on the interface related properties. Our ongoing efforts are to carry out systematic studies on the effects of other experimental parameters, including the reaction temperature, time and the concentration of all the reactants involved.

3.4. Formation mechanism in Pocket Cubes of $ZnSn(OH)_6$

At the initial stage, nucleation takes place and $ZnSn(OH)_6$ nanoparticles were formed *via* the co-precipitation reaction (Scheme 2a). Then, small cubic particles were formed starting from $ZnSn(OH)_6$ nanoseeds under the conditions where the supersaturation on the surface was practically constant and equal to that in the bulk of the mother liquor (Scheme 2b).[27] As a typical perovskite-structured hydroxide, the evenly distributed Sn and Zn atoms in the $ZnSn(OH)_6$ structure are octahedrally coordinated with O atoms and the formed polyhedra sharing their O atoms as corners. $ZnSn(OH)_6$ with face-centered-cubic closed packing could form a cubic structure under the right conditions. As the crystals grow to microscale dimensions and consume the reactants, the supersaturation over the central parts of the faces may be lower as compared to that over the edges and vertices, leading to the growth along the vertices which is faster than the growth at the center of face. Faces with a pit at the center of the face were generated (Scheme 2c). With prolonged reaction time, progressive deepening of the pit takes place by smooth curving of the face (Scheme 2c). The proposed formation mechanism illustrated in Scheme 2 is also supported by experimental evidence, where small cubes and large Pocket Cubes were observed (Fig. S3 in the ESI†). We observed that, experimentally, the amount of metallic cations introduced could significantly determine the final products in the forms of cubic structures or Pocket Cube structures. When the concentrations of $ZnCl_2$ and $SnCl_4$ were the same at a ratio of 1 : 1, cubic microframes were observed. Cubic particles are also formed in excess Zn^{2+} ($ZnCl_2$ and $SnCl_4$ at a concentration of 0.05 M and 0.025 M, respectively). In contrast, Pocket Cubes are formed in excess Sn^{4+} ($ZnCl_2$ and $SnCl_4$ at a concentration of 0.025 M and 0.045 M, respectively). It was reported that the concentration of $AlCl_3$ as additives can significantly change the morphology of the AgCl microparticle obtained.[28] In our case, the excessive amount of $SnCl_4$ could play a similar role to $AlCl_3$ in changing the morphology of the $ZnSn(OH)_6$ microparticles obtained. However, further studies are required to gain better formation mechanism understanding.

3.5. Morphology of the 2 × 2 × 2 Pocket Cubes of Zn_2SnO_4&SnO_2

Microscale Pocket Cubes of Zn_2SnO_4&SnO_2 were obtained by calcinating the $ZnSn(OH)_6$ precursor. As shown in Fig. 4, the secondary Pocket microcube structure was maintained after thermal decomposition. The preserved Pocket Cube-like structure suggests good structural stability of the obtained composites of Zn_2SnO_4&SnO_2 under higher temperature calcination (Fig. 4a and b). The depression on each facets is also preserved (Fig. 4c), but the surface of the microstructure is much coarser indicting that the basic building units are the nanoparticles. The size of the primary nanoparticles is in agreement with the estimated crystalline sizes based on the Scherrer equation from the XRD analysis. Therefore, the $ZnSn(OH)_6$ precursor can be used to generate the nanoparticle aggregates with evenly distributed Zn_2SnO_4 and SnO_2 nanoparticles as the basic building units but still with the unique Pocket Cube-like microscale structure. The microparticles are highly porous due to the loosely aggregated nanoparticle building units in the Pocket Cubes (Fig. 4d)

3.6. Morphology of the 2 × 2 × 2 Pocket Cubes of Zn_2SnO_4&Sn@C

In another example, we demonstrate that the Zn_2SnO_4&Sn@C Pocket Cubes could be prepared from the highly porous Pocket Cubes of Zn_2SnO_4&SnO_2 nanoparticle aggregates as the precursor. The gaps or nanopores generated between nanoparticle aggregates can facilitate the diffusion of C_2H_2 gas into the microstructure. CVD was carried out to coat the carbon layer on the secondary microstructure as well as the primary nanoparticles. The carbon coating outside the structure can serve as the conducting layer and also buffer layer

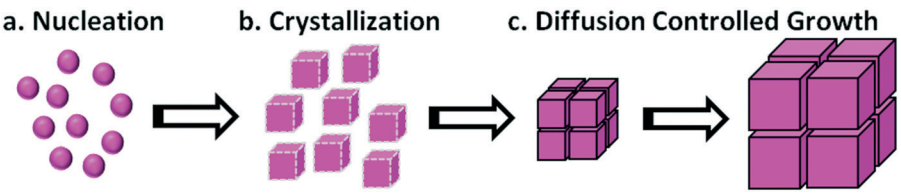

Scheme 2 Illustration of the proposed plausible mechanism of the formation of Pocket Cubes: (a) initial nucleation forming nanoparticles; (b) nanocubes formed based on seeded growth; (c) formation of a Pocket Cube *via* diffusion controlled growth leading to anisotropic growth; further growth, Ostwald ripening and NaOH etching could all contribute to the final product Pocket Cubes.

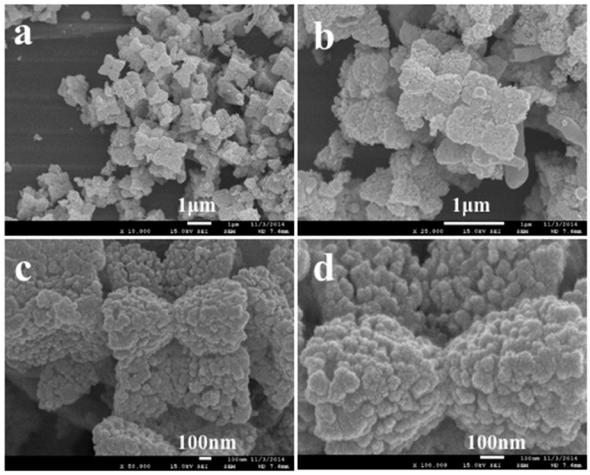

Fig. 4 FESEM images of the Zn_2SnO_4&SnO_2 Pocket Cubes prepared *via* the calcination of the $ZnSn(OH)_6$ precursor: (a) overall-view, (b) a few representative Pocket Cubes, (c) single Pocket Cube showing the detailed structure, and (d) high-magnification image showing the building units.

for energy storage applications.[29] It also allows the preparation of hollow carbon structures, which have various applications such as catalyst supports,[30] gas storage, coating, and sensors, as well as in separation.[31] SnO_2 was reduced to metallic tin by C_2H_2, as proved by XRD. After the CVD process, the overall Pocket Cube-like morphology with the secondary microstructure and primary nanoparticles was well maintained (Fig. 5a and b). The size of the primary nanoparticles is similar to the size of the primary nanoparticle of Zn_2SnO_4&SnO_2 (Fig. 5c and d). A few nanorods were observed, which might be the carbon nanorods formed with Sn as the catalyst, which has been documented before.[23,32]

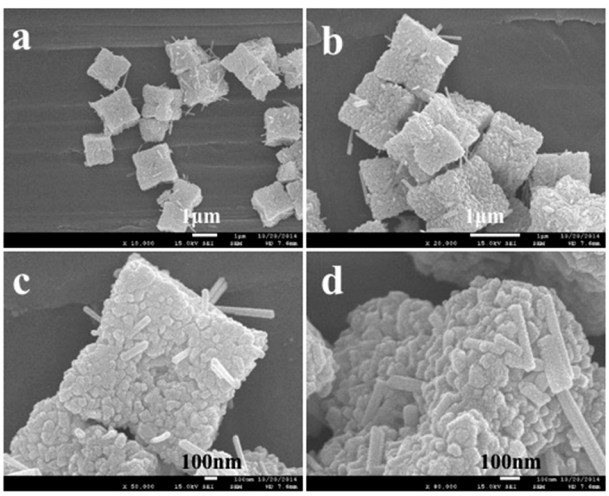

Fig. 5 FESEM images of the Zn_2SnO_4&Sn@C Pocket Cubes prepared *via* CVD of the Zn_2SnO_4&SnO_2 Pocket Cubes: (a) overall-view, (b) a few representative Pocket Cubes, (c) single Pocket Cube structure showing the details and (d) high-magnification image showing the building units.

3.7. Morphology of the 2 × 2 × 2 Pocket Cubes of carbon nanobubbles

Acid treatment was carried out to remove the cores consisting of Zn_2SnO_4 and Sn encapsulated inside of the carbon sheath. The derived carbon structure was revealed by FESEM (Fig. 6). Zn^{2+} and metallic Sn can be removed in the form of soluble salts $ZnCl_2$ and $SnCl_2$/$SnCl_4$. H_4SnO_4 would form *via* the reaction between H^+ and SnO_4^{4+}, which may further react with HCl.[33,34] After the removal of the nanoparticle core, the secondary Pocket microcube structure can still be preserved (Fig. 6a and b). And the shape of the primary particles was also inherited from Zn_2SnO_4&Sn@C, with hollow C bubbles as the primary building units (Fig. 6c and d). The nanobubble structure can be more clearly revealed by TEM (Fig. 6e and f). The whole microstructure was in shallow color, indicating the successful removal of Zn_2SnO_4 and Sn cores by acid and the formation of nanobubble assemblies (Fig. 6e). Only a few dark dots were observed, which came from the Zn_2SnO_4 or Sn nanoparticle residues. The C nanobubbles are 30–60 nm in size, which is similar to the size of Zn_2SnO_4 and Sn calculated from XRD and Zn_2SnO_4&Sn@C

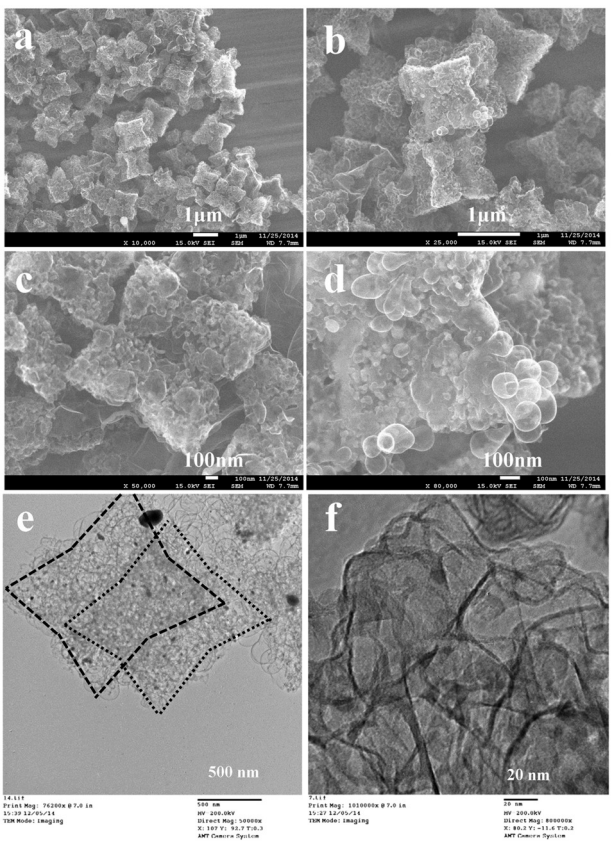

Fig. 6 FESEM images of the Pocket microcubes of C nanobubble assemblies prepared *via* the acid treatment of the Zn_2SnO_4&Sn@C Pocket microcube: (a) overall-view, (b) a few representative Pocket Cubes, (c) single Pocket Cube structure showing the detailed structure and (d) high-magnification image showing the building units. (e and f) TEM images of final product Pocket Cube-like carbon nanobubble aggregates. Dashed lines in (e) highlight two carbon Pocket Cubes.

from FESEM, and the thickness of the carbon layer is ~3 nm (Fig. 6f). The formation of carbon bubbles indicates that C_2H_2 diffused *via* the nanopores, and the carbon layer was coated on all the primary nanoparticles inside the Pocket Cubes. Thus, we have successfully prepared C nanobubble assemblies which inherited the secondary Pocket microcube structure from its precursor. This unique hierarchical microstructure with theoretically high surface area may favor its application in energy storage,[35] catalysis,[36] drug delivery,[37] *etc.* It is also possible to use diluted acid to partially remove the Zn_2SnO_4&Sn from Zn_2SnO_4&Sn@C, for obtaining the secondary Pocket microcube structure with SnO_2@C nanobubbles as the primary building units, which is part our ongoing efforts.

3.8. Photocatalytic application of the Pocket Cubes

In order to preliminarily evaluate the potential applications of this family of Pocket Cubes, we investigated the photocatalytic performance of one of the family members, the Pocket Cubes of Zn_2SnO_4&SnO_2, in wastewater treatment (Fig. 7). Methylene blue (MB) was selected as the model organic contaminant in wastewater, and it can be easily monitored in water. UV-visible absorption spectroscopy was used to record the photo-degradation behaviors of the microscale Pocket Cubes of Zn_2SnO_4&SnO_2. Fig. 7a shows the time-dependent absorption spectra of the MB solution. The characteristic absorption of MB at approximately 663 nm was used to monitor the photo-degradation process for MB. To reveal the degradation behavior of the Pocket microcubes, the C/C_0 *vs.* reaction time was plotted (Fig. 7b). Here, C_0 and C are the concentrations of MB at 0 minute (right before it was exposed to UV light after being kept in the dark for 15 min). The concentration change in the dark is insignificant after 15 minute. In contrast, the MB concentration decreased rapidly under the UV treatment, which demonstrated the capability of the Zn_2SnO_4&SnO_2 Pocket microcubes to photocatalytically degrade MB. 91.2% of MB was degraded in just 27 minutes. The control experiment without the presence of Zn_2SnO_4&SnO_2 microparticles under the same UV-light treatment is shown in Fig. S4 in the ESI.† The control experiment demonstrated that the degradation of MB without any photocatalyst was not significant after the same exposure time. The $\ln(C/C_0)$ *vs.* t plot was linear, indicating the 1st order reaction kinetics (Fig. 7c). The rate constant of the de-colorization (k) was estimated to be 0.04442 min^{-1}. This rate constant is higher than that of Zn_2SnO_4 particles, k = 0.0326 min^{-1},[38] and significantly higher than that of SnO_2 quantum dots, k = 0.0002–0.0095 min^{-1}.[39] The improved performances could be attributed to the porous nature of the mixed oxides in those microscale Pocket Cubes. We believe that additional optimization can further improve the photocatalytic performances of our Pocket Cubes of Zn_2SnO_4&SnO_2 microparticles in the treatment of other organic compounds, which will require further studies.

3.9. Application of the Pocket Cubes in batteries

In another proof-of-concept demonstration, we investigated another family member, the Pocket Cubes of carbon bubble assemblies, for their application in sodium-ion batteries (Fig. 8). Different from the Li-ion storage, no significant amount of Na ions can be reversibly stored in graphite (less than 5 mA h g^{-1}), which is widely used as the anode in Li-ion batteries.[40] There is increasing interest in the development of various types of carbon materials, besides graphite, for the reversible storage of Na ions. For example, hard carbon and amorphous carbon have been reported to reversibly store a significant amount of Na ions (more than 100 mA h g^{-1}).[40–42] Nanostructured carbon materials are promising candidates for sodium-ion batteries.[42] The Pocket Cubes of the carbon bubble assemblies are mainly in the amorphous state, as evidenced by the lack of graphite peaks in the XRD analysis (Fig. 1c).[43] The defects and disorders are expected to be beneficial to the Na-ion storage.

The initial charge–discharge profile is shown in Fig. 8a. The first-cycle discharge capacity (sodium insertion) was 1080 mA h g^{-1}. However, the first cycle irreversible capacity loss was huge, 907 mA h g^{-1}. The first cycle Coulombic efficiency was low,16%. The irreversible capacity loss is

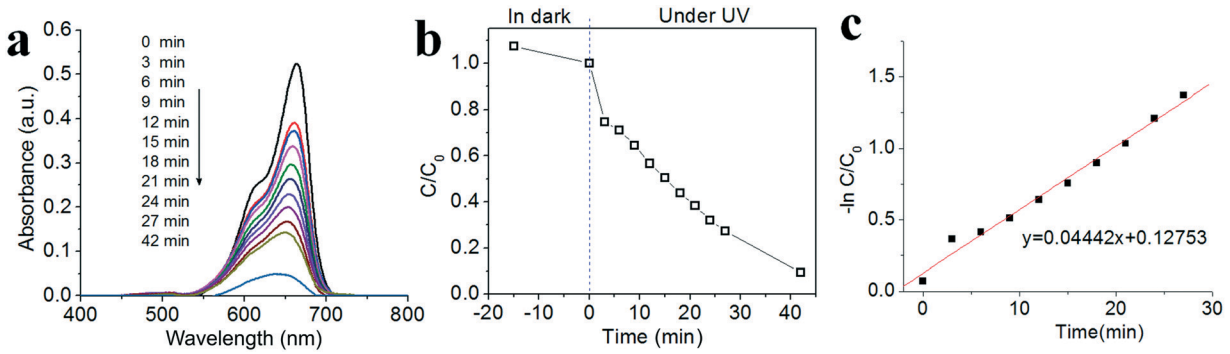

Fig. 7 (a) UV-vis absorption spectra of the methylene blue (MB) solution (6 μM, 60 mL) in the presence of 60 mg Pocket Cubes of the Zn_2SnO_4&SnO_2 microparticles at an interval of 3 min after the exposure to UV-visible light, (b) MB normalized concentration *vs.* the treatment time plot, and (c) photocatalytic reaction kinetics of MB with the reaction time plot.

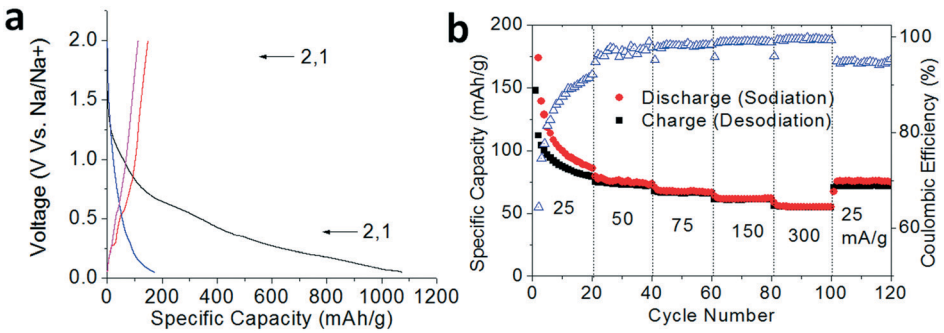

Fig. 8 (a) Charge–discharge profiles for the first two cycles and the (b) cycling performance and Coulombic efficiency of the Pocket microcubes of the carbon nanobubble assemblies as the anode materials for Na-ion batteries.

attributed to the high surface area and decomposition of electrolytes at the surface of the electrodes and the formation of solid-electrolyte interphase. The Coulombic efficiency was improved to 99.5% at the 82th cycle, indicating the highly reversible sodium ion insertion and extraction (Fig. 8b). Interestingly, the Pocket Cubes of the carbon bubble assemblies demonstrated reasonable rate performance when the testing currents were increased (Fig. 8b). The capacities measured were 79, 72, 66, 61, and 55 mA h g^{-1} at the testing currents from 25 to 300 mA g^{-1}. The capacity was recovered to 71 mA h g^{-1} after the current was changed back to 25 mA g^{-1}. The capacity at a high testing current of 300 mA g^{-1} was about 70% of the capacity obtained at an initial testing current of 25 mA g^{-1}, indicating a relatively good rate performance. This good rate performance may be attributed to the good electric conductivity and interconnection of the C nanobubbles. Other members of this family of microscale Pocket Cubes were also preliminarily evaluated for lithium-ion batteries, demonstrating their activity in reversible lithium ion storage (Fig. S5 in the ESI†). Although the preliminary results suggest that their electrochemical performances are not very good, one should note that our Pocket Cube-like particles are on the microscale instead of nanoscale. We believe that electrochemical performances of those microscale Pocket Cubes could be further improved and optimized, which is part of our ongoing efforts.

4. Conclusion

We report a facile procedure to prepare a family of microscale Pocket Cubes of nanoparticle aggregates on a large scale. Our results suggest that it is possible to synthesize microscale Pocket Cubes and tune their compositions and properties. This family of microscale Pocket Cubes of different chemical compositions will provide a rich pool of materials to meet the demands in different applications. We preliminarily demonstrated that those family members of microscale Pocket Cubes could find applications in photocatalysis and batteries. Our results suggest that microscale particles could demonstrate comparable photocatalytic properties to nanoparticles. The family of microscale Pocket Cubes could find applications in both sodium- and lithium-ion batteries. Our ongoing effort is to further optimize their performances and gain better fundamental understanding.

Author contributions

Deng conceived the idea and supervised the research. Aldossary, Zhu and Porob conducted the experiments. All the authors participated in the manuscript writing and revision.

Acknowledgements

The authors thank Prof. Stephanie Brock for helpful discussion.

References

1 S. J. Shi, Z. R. Lou, T. F. Xia, X. L. Wang, C. D. Gu and J. P. Tu, Hollow $Li_{1.2}Mn_{0.5}Co_{0.25}Ni_{0.05}O_2$ Microcube Prepared by Binary Template as a Cathode Material for Lithium Ion Batteries, *J. Power Sources*, 2014, **257**, 198–204.
2 N. Feng, S. Peng, X. Sun, L. Qiao, X. Li, P. Wang, D. Hu and D. He, Synthesis of Monodisperse Single Crystal Zn2sno4 Cubes with High Lithium Storage Capacity, *Mater. Lett.*, 2012, **76**, 66–68.
3 J. Bai, X. Li, G. Liu, Y. Qian and S. Xiong, Unusual Formation of $ZnCo_2O_4$ 3D Hierarchical Twin Microspheres as a High-Rate and Ultralong-Life Lithium-Ion Battery Anode Material, *Adv. Funct. Mater.*, 2014, **24**, 3012–3020.
4 S. Zeng, K. Tang, T. Li, Z. Liang, D. Wang, Y. Wang and W. Zhou, Hematite Hollow Spindles and Microspheres: Selective Synthesis, Growth Mechanisms, and Application in Lithium Ion Battery and Water Treatment, *J. Phys. Chem. C*, 2007, **111**, 10217–10225.
5 I. Stambolova, K. Konstantinov, D. Kovacheva, P. Peshev and T. Donchev, Spray Pyrolysis Preparation and Humidity Sensing Characteristics of Spinel Zinc Stannate Thin Films, *J. Solid State Chem.*, 1997, **128**, 305–309.
6 J. H. Yu and G. M. Choi, Selective Co Gas Detection of Zn_2SnO_4 Gas Sensor, *J. Electroceram.*, 2002, **8**, 249–255.
7 J. H. Yu and G. M. Choi, Current–Voltage Characteristics and Selective Co Detection of Zn_2SnO_4 and Zno/Zn_2SnO_4, SnO_2/Zn_2SnO_4 Layered-Type Sensors, *Sens. Actuators, B*, 2001, **72**, 141–148.

8 J. Wang, H. Li, S. Meng, L. Zhang, X. Fu and S. Chen, One-Pot Hydrothermal Synthesis of Highly Efficient Snox/Zn_2SnO_4 Composite Photocatalyst for the Degradation of Methyl Orange and Gaseous Benzene, *Appl. Catal., B*, 2017, **200**, 19–30.
9 D. Arcos, A. López-Noriega, E. Ruiz-Hernández, O. Terasaki and M. Vallet-Regí, Ordered Mesoporous Microspheres for Bone Grafting and Drug Delivery, *Chem. Mater.*, 2009, **21**, 1000–1009.
10 M. Yin, F. Wang, H. Fan, L. Xu and S. Liu, Heterojunction Cuo@Zno Microcubes for Superior P-Type Gas Sensor Application, *J. Alloys Compd.*, 2016, **672**, 374–379.
11 Z. Li, Y. Zhou, J. Zhang, W. Tu, Q. Liu, T. Yu and Z. Zou, Hexagonal Nanoplate-Textured Micro-Octahedron Zn2sno4: Combined Effects toward Enhanced Efficiencies of Dye-Sensitized Solar Cell and Photoreduction of CO_2 into Hydrocarbon Fuels, *Cryst. Growth Des.*, 2012, **12**, 1476–1481.
12 S. K. Addu, J. Zhu, K. Y. S. Ng and D. Deng, A Family of Mesocubes, *Chem. Mater.*, 2014, **26**, 4472–4485.
13 H. Zhu, D. Yang, G. Yu, H. Zhang, D. Jin and K. Yao, Hydrothermal Synthesis of Zn_2SnO_4 Nanorods in the Diameter Regime of Sub-5 nm and Their Properties, *J. Phys. Chem. B*, 2006, **110**, 7631–7634.
14 Z. Chen, M. Cao and C. Hu, Novel Zn2sno4 Hierarchical Nanostructures and Their Gas Sensing Properties toward Ethanol, *J. Phys. Chem. C*, 2011, **115**, 5522–5529.
15 S. Danwittayakul, M. Jaisai and J. Dutta, Efficient Solar Photocatalytic Degradation of Textile Wastewater Using ZnO/ZTO Composites, *Appl. Catal., B*, 2015, **163**, 1–8.
16 H. Chen, J. Wang, H. Yu, H. Yang, S. Xie and J. Li, Transmission Electron Microscopy Study of Pseudoperiodically Twinned Zn_2SnO_4 Nanowires, *J. Phys. Chem. B*, 2005, **109**, 2573–2577.
17 J.-B. Shi, P.-F. Wu, H.-S. Lin, Y.-T. Lin, H.-W. Lee, C.-T. Kao, W.-H. Liao and S.-L. Young, Synthesis and Characterization of Single-Crystalline Zinc Tin Oxide Nanowires, *Nanoscale Res. Lett.*, 2014, **9**, 210.
18 Y. Li and X. L. Ma, Nanobelts and Nanocones of Spinel Zn_2SnO_4, *Phys. Status Solidi A*, 2005, **202**, 435–440.
19 L. Sun, X. Han, Z. Jiang, T. Ye, R. Li, X. Zhao and X. Han, Fabrication of Cubic Zn_2SnO_4/SnO_2 Complex Hollow Structures and Their Sunlight-Driven Photocatalytic Activity, *Nanoscale*, 2016, **8**, 12858–12862.
20 B. Li, L. Luo, T. Xiao, X. Hu, L. Lu, J. Wang and Y. Tang, Zn_2SnO_4–SnO_2 Heterojunction Nanocomposites for Dye-Sensitized Solar Cells, *J. Alloys Compd.*, 2011, **509**, 2186–2191.
21 S. H. Lee, M. Mathews, H. Toghiani, D. O. Wipf and J. C. U. Pittman, Fabrication of Carbon-Encapsulated Mono- and Bimetallic (Sn and Sn/Sb Alloy) Nanorods, Potential Lithium-Ion Battery Anode Materials, *Chem. Mater.*, 2009, **21**, 2306–2314.
22 D. Deng, M. G. Kim, J. Y. Lee and J. Cho, Green Energy Storage Materials: Nanostructured Tio 2 and Sn-Based Anodes for Lithium-Ion Batteries, *Energy Environ. Sci.*, 2009, **2**, 818–837.
23 D. Deng and J. Y. Lee, Direct Fabrication of Double-Rough Chestnut-Like Multifunctional Sn@C Composites on Copper Foil: Lotus Effect and Lithium Ion Storage Properties, *J. Mater. Chem.*, 2010, **20**, 8045–8049.
24 J. Yin, F. Gao, C. Wei and Q. Lu, Controlled Growth and Applications of Complex Metal Oxide $ZnSn(OH)_6$ Polyhedra, *Inorg. Chem.*, 2012, **51**, 10990–10995.
25 L. Han, J. Liu and Z. Wang, *et al.*, Shape-Controlled Synthesis of $ZnSn(OH)_6$ Crystallites and Their Hcho-Sensing Properties, *CrystEngComm*, 2012, **14**, 3380–3386.
26 L. Wang, K. Tang, Z. Liu, D. Wang, J. Sheng and W. Cheng, Single-Crystalline $ZnSn(OH)_6$ Hollow Cubes Via Self-Templated Synthesis at Room Temperature and Their Photocatalytic Properties, *J. Mater. Chem.*, 2011, **21**, 4352–4357.
27 A. A. Chernov, *Modern Crystallography III-Crystal Growth*, Springer-Verlag, Berlin Heidelberg, 1984.
28 H. Daupor and S. Wongnawa, Flower-Like Ag/AgCl Microcrystals: Synthesis and Photocatalytic Activity, *Mater. Chem. Phys.*, 2015, **159**, 71–82.
29 R. Zou, M. F. Yuen, L. Yu, J. Hu, C.-S. Lee and W. Zhang, Electrochemical Energy Storage Application and Degradation Analysis of Carbon-Coated Hierarchical $NiCo_2S_4$ Core-Shell Nanowire Arrays Grown Directly on Graphene/Nickel Foam, *Sci. Rep.*, 2016, **6**, 20264.
30 R. Liu, S. M. Mahurin, C. Li, R. R. Unocic, J. C. Idrobo, H. Gao, S. J. Pennycook and S. Dai, Dopamine as a Carbon Source: The Controlled Synthesis of Hollow Carbon Spheres and Yolk-Structured Carbon Nanocomposites, *Angew. Chem., Int. Ed.*, 2011, **50**, 6799–6802.
31 S. B. Yoon, K. Sohn, J. Y. Kim, C. H. Shin, J. S. Yu and T. Hyeon, Fabrication of Carbon Capsules with Hollow Macroporous Core/Mesoporous Shell Structures, *Adv. Mater.*, 2002, **14**, 19–21.
32 Y. Zou and Y. Wang, Sn@CNT Nanostructures Rooted in Graphene with High and Fast Li-Storage Capacities, *ACS Nano*, 2011, **5**, 8108–8114.
33 J. Xu, C. Zhang, H. Qu and C. Tian, Zinc Hydroxystannate and Zinc Stannate as Flame-Retardant Agents for Flexible Poly(Vinyl Chloride), *J. Appl. Polym. Sci.*, 2005, **98**, 1469–1475.
34 A. T. Al-Hinai, M. H. Al-Hinai and J. Dutta, Application of Eh-Ph Diagram for Room Temperature Precipitation of Zinc Stannate Microcubes in an Aqueous Media, *Mater. Res. Bull.*, 2014, **49**, 645–650.
35 Z. Sun, X. Song, P. Zhang and L. Gao, Template-Assisted Synthesis of Multi-Shelled Carbon Hollow Spheres with an Ultralarge Pore Volume as Anode Materials in Li-Ion Batteries, *RSC Adv.*, 2015, **5**, 3657–3664.
36 J. Wu, C. Jin, Z. Yang, J. Tian and R. Yang, Synthesis of Phosphorus-Doped Carbon Hollow Spheres as Efficient Metal-Free Electrocatalysts for Oxygen Reduction, *Carbon*, 2015, **82**, 562–571.
37 Y. Li, Y. Yang, J. Shi and M. Ruan, Synthesis and Characterization of Hollow Mesoporous Carbon Spheres with a Highly Ordered Bicontinuous Cubic Mesostructure, *Microporous Mesoporous Mater.*, 2008, **112**, 597–602.

38 M. Najam Khan, M. Al-Hinai, A. Al-Hinai and J. Dutta, Visible Light Photocatalysis of Mixed Phase Zinc Stannate/Zinc Oxide Nanostructures Precipitated at Room Temperature in Aqueous Media, *Ceram. Int.*, 2014, **40**, 8743–8752.
39 X. Liu, L. Pan, T. Chen, J. Li, K. Yu, Z. Sun and C. Sun, Visible Light Photocatalytic Degradation of Methylene Blue by Sno2 Quantum Dots Prepared Via Microwave-Assisted Method, *Catal. Sci. Technol.*, 2013, **3**, 1805–1809.
40 M. D. Slater, D. Kim, E. Lee and C. S. Johnson, Sodium-Ion Batteries, *Adv. Funct. Mater.*, 2013, **23**, 947–958.
41 R. Alcántara, J. M. Jiménez-Mateos, P. Lavela and J. L. Tirado, Carbon Black: A Promising Electrode Material for Sodium-Ion Batteries, *Electrochem. Commun.*, 2001, **3**, 639–642.
42 Y. Cao, L. Xiao and M. L. Sushko, *et al.*, Sodium Ion Insertion in Hollow Carbon Nanowires for Battery Applications, *Nano Lett.*, 2012, **12**, 3783–3787.
43 J. Ji, H. Ji, L. L. Zhang, X. Zhao, X. Bai, X. Fan, F. Zhang and R. S. Ruoff, Graphene-Encapsulated Si on Ultrathin-Graphite Foam as Anode for High Capacity Lithium-Ion Batteries, *Adv. Mater.*, 2013, **25**, 4673–4677.